

Spaceborne Imaging Radar: Geologic and Oceanographic Applications

Charles Elachi

In June 1978, the Seasat satellite was put into orbit around the earth with a payload of active microwave sensors consisting of an altimeter, a scatterometer, and an imaging synthetic aperture radar (SAR). The objective of the mission was a proof-of-concept demonstration of the capability to monitor the ocean sur-

face and near-surface features such as surface waves, internal waves, currents, eddies, surface wind, surface topography, and ice cover (1). The imaging radar, which was operated in the synthetic aperture mode (2, 3), provided, for the first time, synoptic radar images of the earth's surface (both ocean and land areas) obtained from an orbiting platform. The resolution of these images is about 25 meters. The success of this complex sensor was a major technological advance, and it opened up a new dimension in our capability to observe, monitor, and study the earth's surface.

from the sun. The radar energy also penetrates cloud cover; consequently, the sensor operation is not constrained by weather conditions. The illumination angle and illumination direction can be controlled and selected (4), whereas in optical systems these parameters are constrained by the sun's location. The

Summary. Synoptic, large-area radar images of the earth's land and ocean surface, obtained from the Seasat orbiting spacecraft, show the potential for geologic mapping and for monitoring of ocean surface patterns. Structural and topographic features such as lineaments, anticlines, folds and domes, drainage patterns, stratification, and roughness units can be mapped. Ocean surface waves, internal waves, current boundaries, and large-scale eddies have been observed in numerous images taken by the Seasat imaging radar. This article gives an illustrated overview of these applications.

The SAR imaging sensor has some unique characteristics. It is an active system; that is, it uses its own energy to illuminate the surface, and it generates an image from the backscatter echoes. Thus it is not dependent on illumination

trial organizations use airborne radar images for large-scale mapping, particularly in equatorial regions with extensive cloud cover. Almost all of Brazil, Nigeria, Venezuela, Panama, Togo, and several other countries in the tropical regions, as well as many areas in the United States, have been mapped with radar, some for the first time (5).

Most of the radar imaging of the ocean surface in the past has been experimental in nature (6-10). Before the advent of Seasat, airborne SAR sensors had been used to image surface waves, internal waves, currents, weather fronts, polar ice (11), and ocean vessels. However, the usefulness of these observations was severely hindered by the limited temporal and spatial extent that could be achieved with an airborne platform. The Seasat SAR demonstrated that numerous ocean surface features can be observed and potentially monitored from a space platform that can provide synoptic coverage of large areas and fast repetitive observations of a particular region.

Exploration companies, government agencies, geological surveys, and indus-

The Seasat SAR provided, for the first time, synoptic radar images of large areas with a homogeneous illumination geometry. Each Seasat SAR data path covers an area 100 kilometers wide and about 4000 km long with a resolution of 25 m. The incidence angle at the surface was about $20^\circ \pm 3^\circ$ from the vertical. The orbit inclination was 108° , which allowed two illumination directions (one during the ascending pass and one during the descending pass) for specific regions.

The Seasat SAR was designed to observe the ocean surface where there is little topography. However, it also provided useful images of large land regions in the continental United States, Canada, Alaska, Central America, and Western Europe. The land images are most useful in regions with low to moderate relief. In rugged mountainous regions, the foldover effect (12) gives exaggerated distortion, which complicates the interpretation of the image.

The purpose of this article is to give an overview of the characteristics and po-

The author heads the Radar Remote Sensing Group in the Earth and Space Sciences Division at the Jet Propulsion Laboratory, California Institute of Technology, Pasadena 91103.

tential applications of spaceborne imaging radar, particularly in geology and oceanography. The synthetic aperture technique and the unique requirements of spaceborne SAR sensors are reviewed first. Then I discuss the different applications of spaceborne radars in geologic mapping, using illustrations from the Seasat SAR images. The oceanographic applications are discussed next. The analysis of the Seasat SAR data is still at an early stage, and most of the discussions presented here are preliminary. A number of radar images are included, with only a brief discussion, to give the reader a broad idea of the different features that can be observed. All of the figures (except Fig. 1) were obtained with the Seasat SAR.

The SAR Concept

In the synthetic aperture technique, the Doppler information in the returned echo is used simultaneously with the time delay information to generate a high-resolution image of the surface being illuminated by the radar. The radar usually "looks" to one side of the moving platform (to eliminate right-left ambiguities) and perpendicular to its line of motion. It transmits a short pulse of coherent electromagnetic energy toward the surface. Points equidistant from the radar are located on successive concentric spheres. The intersection of these spheres with the surface gives a series of concentric circles centered at the nadir point (Fig. 1). The backscatter echoes from objects along a certain circle will have a well-defined time delay.

Points distributed on coaxial cones, with the flight line as the axis and the radar as the apex, provide identical Doppler shifts of the returned echo. The intersection of these cones with the surface gives a family of hyperbolas (Fig. 1). Objects on a specific hyperbola will provide equi-Doppler returns. Thus, if the time delay and Doppler information in the returned echoes are processed simultaneously, the surface can be divided into a coordinate system of concentric circles and coaxial hyperbolas (Fig. 1), and each point on the surface can be uniquely identified by a specific time delay and specific Doppler. The brightness that is assigned to a specific pixel (picture resolution element) in the radar image is proportional to the echo energy contained in the time delay bin and Doppler bin which corresponds to the equivalent point on the surface being imaged. The

resolution capability of the imaging system is thus dependent on the measurement accuracy of the differential time delay and differential Doppler (or phase) between two neighboring points on the surface.

In actuality, the situation is somewhat more complicated. The radar transmits a pulsed signal which is necessary to obtain the time delay information. To obtain the Doppler information unambiguously, the echoes from many pulses are required to meet the Nyquist (12) sampling criterion. Thus, as the moving platform passes over a certain region, the recorded series of echoes contains a complete Doppler history and range-change history for each point on the surface that is being illuminated. These complete histories are then processed to identify uniquely each point on the surface and to generate the image (2, 12). This is why a very large number of operations is required to generate one pixel in the image; such is not the case in optical sensors. A simplified comparison is that the radar sensor generates the equivalent of a hologram of the surface, and further processing is required to obtain the image. This processing can be done either optically or digitally.

In the case of spaceborne sensors, there are additional effects (3) that are not encountered with airborne sensors. (i) The rotation of the earth relative to the spacecraft adds a Doppler shift that must be accounted for during processing. This Doppler shift varies as a function of latitude and inclination of the orbit. (ii) The orbit eccentricity causes an altitude rate of change which translates into a Doppler shift that must be eliminated. (iii) The ionospheric granularities introduce

phase scintillations which induce errors in the Doppler measurements. (iv) The far distance to the surface requires that many pulses be transmitted before the echo from the first one is received, and attention must be given to the timing of the transmitted and received echoes.

The synthetic aperture imaging technique has one unique characteristic. The resolution capability is dependent on the measurement accuracy, in the range dimension, of the differential time delay between two different points, and in the azimuth dimension of the Doppler shift from a target. Neither of these measurements is related to the absolute distance from the radar to the surface. Thus, the resolution of an imaging SAR is independent of the altitude of the platform (2, 3). Spaceborne and airborne SAR's with similar characteristics will have the same resolution capability. The main difference is that spaceborne sensors require more transmitted power to be able to obtain the necessary echo signal-to-noise ratio. The size of the antenna aperture is usually determined by the width of the swath being imaged and the observing geometry, not by the resolution.

Application in Geologic Mapping

The brightness in the radar image is a representation of the surface backscatter cross section, which is a function of the surface slope, surface roughness at the scale of the observing wavelength, and surface complex dielectric constant. The geologic interpretation of the radar image is based on two general types of information, (i) geometric patterns and shapes and (ii) image tone and texture. Examples of the former are lineaments, joints, folds, domes, drainage pattern density, fracture patterns, and the spatial relationships between these features. These patterns, forms, and shapes are interpreted in a way similar to that used with regular photography (13). The radar technique has the advantage that the angle of illumination and direction of illumination are selectable (4). This is not the case with regular photography where the geometry is fixed by the position of the sun and the time of the year, and some illumination directions are not available at any time of the year. Image tone and texture are primarily a function of the surface roughness and sub-resolution small-scale topography, the surface complex dielectric constant, and surface variations on the scale of few resolution elements. The dielectric property is most useful in the study of vege-

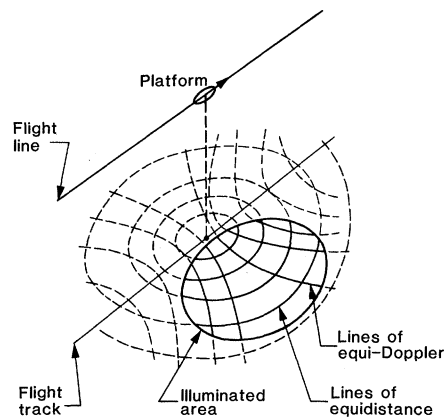


Fig. 1. Constant time delay and Doppler contour lines, which form the radar imaging coordinate system. Each point on the surface can be uniquely identified if the energy in the appropriate time delay bin and Doppler shift bin is filtered out of the received echoes.

tated and moist surfaces. The tonal and textural data in the radar image provide new information that is not available with optical or infrared photography; their interpretation requires an understanding of the interaction of electromagnetic waves, in the microwave region, with natural surfaces.

The sensitivity of the amplitude of the radar echo to changes in the surface topography is very high in comparison to the optical and infrared albedo. A change in the surface slope of a few degrees can easily change the amplitude of the radar echo by a factor of 2 or more, particularly at small incidence angles (up to 30° from the vertical). At larger incidence angles (30° to 70°), the backscattered energy is proportional to the roughness power spectrum, which can easily change by a factor of 10 or more between two neighboring geologic units (14). In comparison, optical albedo rarely changes by more than a factor of 10 (from about 0.06 for basalts to 0.6 for the brightest salts). Thus, the radar sensor is most useful for the study of patterns and features that are expressed in changes of slope or roughness. This is why airborne

radar sensors have been used mostly for geomorphologic and structural mapping (4). Specific examples from the Seasat data will be discussed later in this section.

The surface roughness and dielectric constant are also useful indicators of changes in the surface rock type. Different rock types will erode differently in a similar environment. They also have different dielectric constants. The presence of moisture (because water has a very high dielectric constant) or vegetation could also help in the separation of lithologic units. However, it is not feasible at the present time to use the radar data to identify the surface rock type. In this application, the radar sensor is most useful in discriminating between areas with different rock types, in providing complementary information in conjunction with optical and infrared sensors, and in planning field investigations.

Lineaments, faults, fractures, and contacts. These features are usually expressed on the surface as sharp changes in the surface topography, morphology, or cover (for example, slope change, alignment of hills or valley sections,

small-scale roughness and texture change, alignment of stream segments, or vegetation cover change). All of these features have a strong effect on the radar wave scattering and are observed on the image as a tonal or textural change. Figure 2 shows the Seasat SAR image of the western Mojave, California, where the Garlock and San Andreas faults intersect. Each fault is clearly delineated as a long linear tonal change resulting from the change in the local topography. More subtle lineaments are observed in Fig. 3, which shows the southern Appalachians around Knoxville, Tennessee. This area is almost completely vegetated, and the lineaments represent the alignment of short valley segments. The localized tonal change is predominantly a result of surface slope changes, which, in some cases, may be as much as 30°. Detailed analyses by Ford (15) show that numerous lineaments are observed on the radar image that have not been detected on the Landsat images. Ford, and earlier investigators, have noted that, where a lineament is expressed by a topographic change, it is least well observed when the illumination direction is parallel to

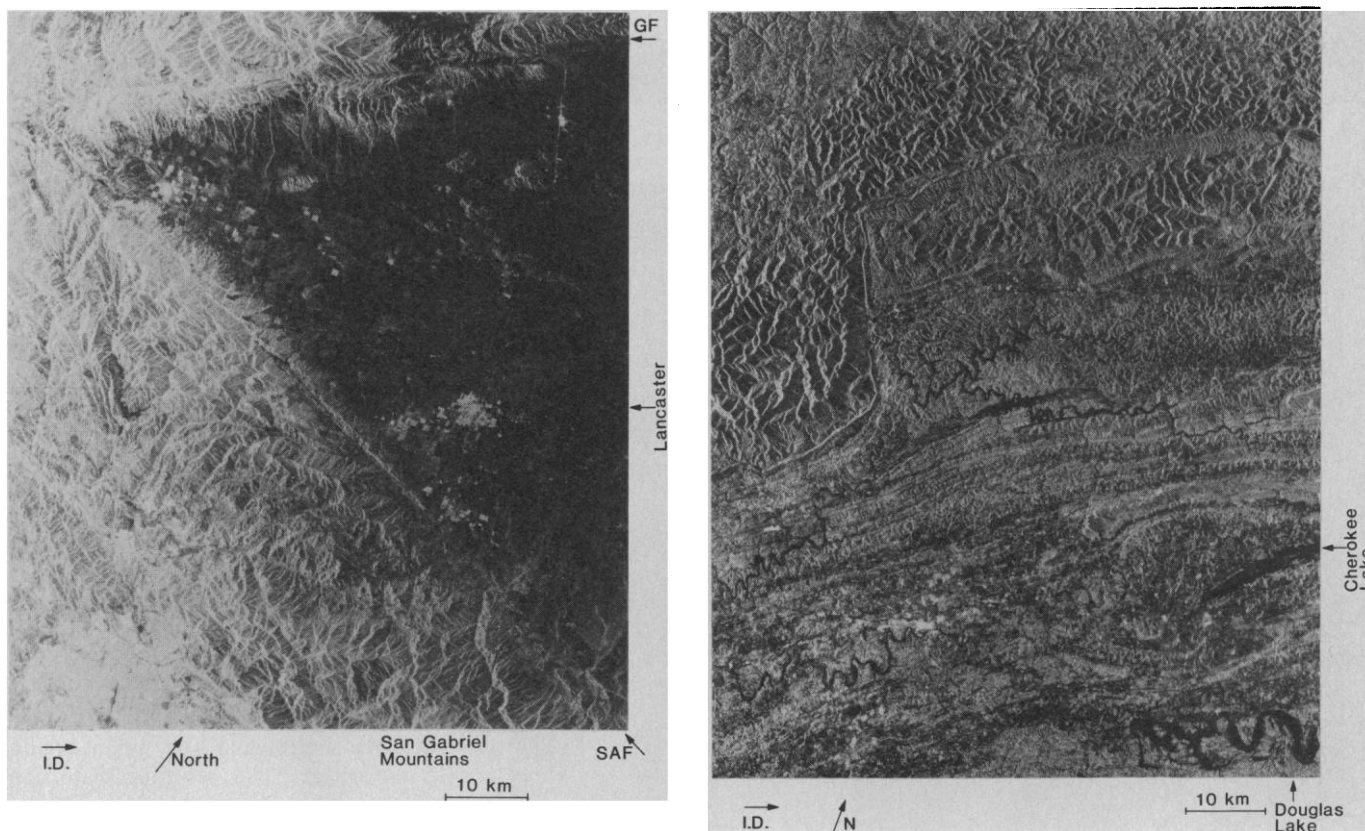


Fig. 2 (left). Radar image of the western Mojave, California (34°50'N, 118°10'W). The San Andreas fault (SAF) and Garlock fault (GF) are visible as abrupt linear tonal changes near the boundary between the bright mountainous region and the dark desert region. Lancaster is the very bright area in the center. The illumination direction is shown by the arrow labeled I.D. Fig. 3 (right). Radar image of the valley and ridge province in northwest Tennessee and the Cumberland plateau in southeastern Kentucky (36°45'N, 83°W). The Pine Mountain overthrust is sharply demarcated across the upper part of the image. The Jacksboro fault at left center marks the southwestern margin of the Pine Mountain thrust block. Tennessee Valley Authority reservoirs are black on the image. Knoxville is the bright region at the bottom left.

the lineament trace. The availability of two different illumination directions from the Seasat SAR substantially reduced this problem (15).

Topographic structural features. Domes, cinder cones, anticlines, synclines, and folds are observed with the radar sensor because of the high sensitivity of the radar return to the slope change. Figure 4a is an image of the Obayos region (northeastern Mexico) where Mesozoic sedimentary rocks have been folded into plunging anticlinal structures. A large breached anticline

and two smaller, doubly plunging anticlines are clearly observed as a result of tonal changes in a recognizable pattern associated with this type of feature. The tonal differences are mainly the result of slope differences which arise from the erosion of dipping beds. Figure 4b shows a folded terrain near Harrisburg, Pennsylvania, which is also observed mainly as a result of topographic expressions from the erosion of different beds.

Sand dune fields. This is another type of geologic feature expressed in terms of local topographic variations. In this

case, the surface is homogeneous and very smooth at the scale of the radar wavelength. The scattering occurs primarily in the specular mode; that is, strong echoes are returned from dune facets that are normal to the incident wave vector. Thus, the radar images mainly the dune with facets which are appropriately oriented relative to the radar illumination. It should be expected then that variations in the image patterns are observed for different illumination directions.

Figure 5 shows two images of the Algodones dunes in southeastern California. The dune patterns are observed mainly as changes in the density of bright specular points. The large barchan dunes in the central region and longitudinal dunes to the west can be identified. The dark areas in the dune field correspond to the interdune flats consisting of relatively smooth gravel pavement. Appreciable variations are observed for the two different illumination directions. The barchan dunes are best identified in Fig. 5b, where the illumination is perpendicular to the crest line. Their visibility is enhanced by the foreshortening and foldover effects (16). The longitudinal dunes are observed well on both images; however, different directional components are emphasized in each image.

Canyons. Canyons such as the Grand Canyon in Arizona represent the extreme in topographic discontinuity. In this case, most of the tonal variation in the image is due to shadowing (17). Figure 6 shows the image of the southern rim of the Grand Canyon near Grand Canyon Village. The major rock formations (Kaibab limestone-Coconino sandstone, Redwall limestone, and Tapeats sandstone) are observed as dark bands in the canyon wall because of the shadow from their vertical profile. Indeed, the imaging geometry of the radar sensor is more favorable than the imaging geometry of optical sensors for observing strata exposed in vertical cliffs (17). Thinner strata are observed in Fig. 7 of the Berufjordur region in eastern Iceland. In this case, strata as thin as 50 m could be detected. Because of the foldover and foreshortening effects (16), the steep sides of the mountains which are oriented toward the radar appear as a very bright region in the image. The resulting distortion makes it impossible to observe details on those sides.

Volcanic lava flows. These are observed mainly because of their small-scale topographic (roughness) characteristics. Lava flows, particularly relatively recent ones, usually have much brighter

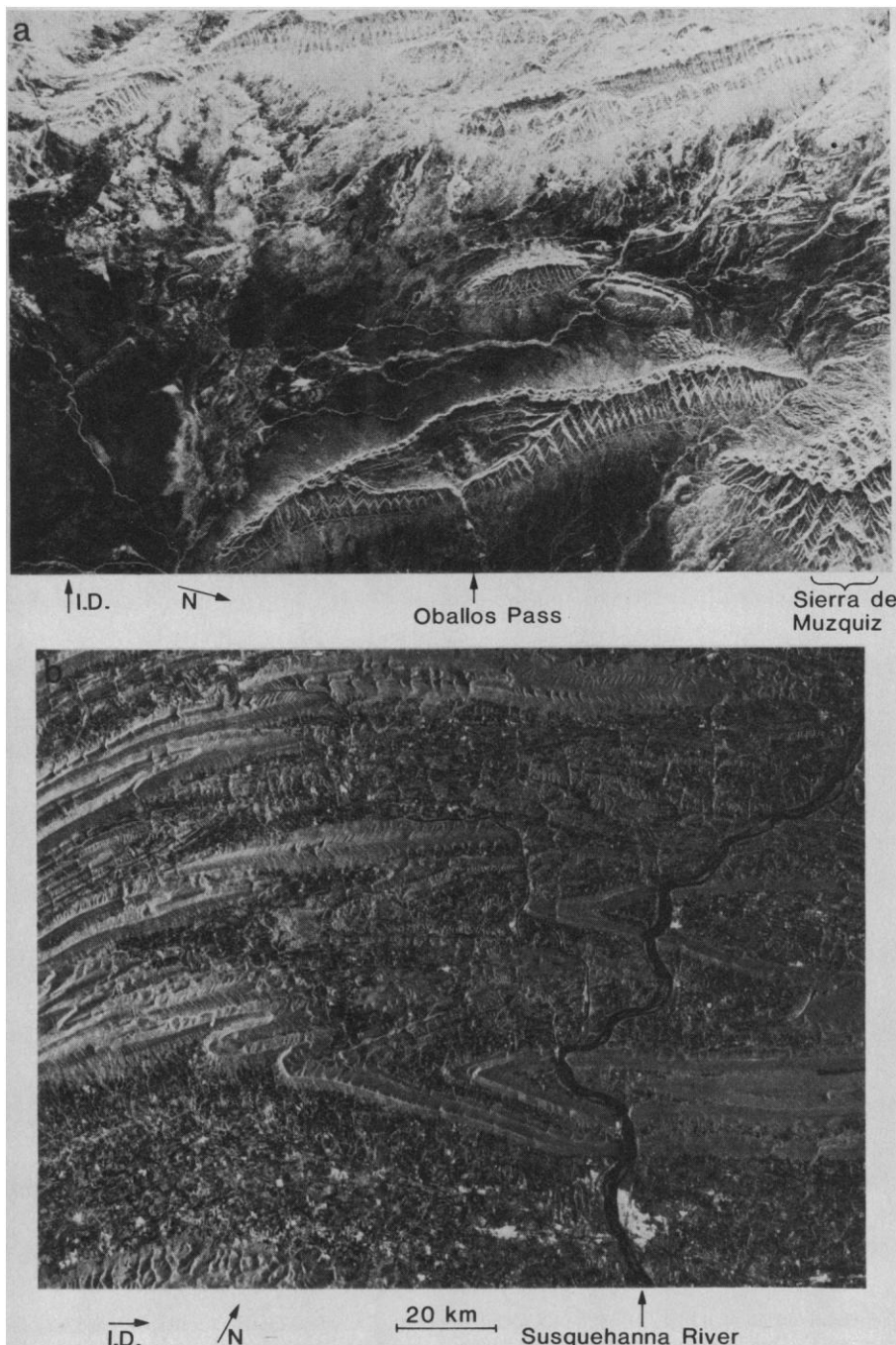


Fig. 4. Examples of topographic structural features. (a) Three plunging anticlines in the Obayos region, Mexico (27°30' N, 101°30' W). (b) Folded terrain in the Harrisburg region of Pennsylvania (40°20' N, 77° W). Harrisburg is seen as a very bright area in the lower part of the image, situated on the bank of the Susquehanna River, which has a dark tone.

tone than their surroundings (see Fig. 6), because their extremely rough surfaces strongly backscatter the radar signal. The tone, form, and surrounding patterns allow us to identify the bright region in the center of Fig. 6 as a lava flow. Almost all the cinder cones and craters in the surrounding regions are also visible on the radar image, as well as the fronts of some older flows. A detailed analysis of the radar imagery of the SP lava flow has been reported by Schaber *et al.* (18).

Drainage patterns. The classification and interpretation of the different drainage patterns observed in a radar image are identical to what is done in photo interpretation (13). Drainage patterns are used to infer variations in the surface lithology (13). In bedrock areas these patterns depend, for the most part, on the lithologic character of the underlying rocks, the attitude of these rock bodies, and the arrangement and spacing of the planes of structural and lithologic weakness encountered by the runoff. Anomalous or abrupt changes in the drainage patterns in the region under observation are particularly important. In the case of the radar sensor, the drainage patterns are observed because of (i) variation in local slope at the edge of a river segment, (ii) variation in vegetation cover, (iii) difference in tone due to the different backscatter from the water surface, and (iv) strong scattering from the boulders and pebbles in the dry channel bottom in arid regions.

Figure 8 shows two examples of Seasat SAR images of drainage patterns in two different environments. Figure 8a shows a region in Pennsylvania, near Lock Haven, where vegetation cover is extensive and the drainage channels are observed primarily as a result of topographic expressions. The drainage pattern density is a good reflection of the lithology of the region. Dense drainage patterns to the north are in the region of the Catskill Formation (red to brown shale and sandstones), which is a relatively soft rock. The drainage pattern in the southern part is less dense. This is a dissected plateau of the Mississippian Pocono Group (conglomerate and sandstone with some shale), which is a relatively resistant rock. The boundary between the two rock types corresponds very closely to the boundary between the two different drainage pattern densities. Figure 8b shows an arid region west of Tucson, Arizona, near Silver Bell, where the drainage channels are observed mostly in terms of riparian vegetation along those channels. Variation in the drainage density is also associated

with variation in the coarseness of the alluvium in that region.

Lithologic mapping. Lithologic mapping cannot be based exclusively on the tonal change in the radar image. The most that can be done is to separate geo-

logic units which have a different surface roughness (which is dependent on the rock type), different susceptibility to moisture content, or different type of vegetation cover. These differences are expressed as a tonal or textural change.

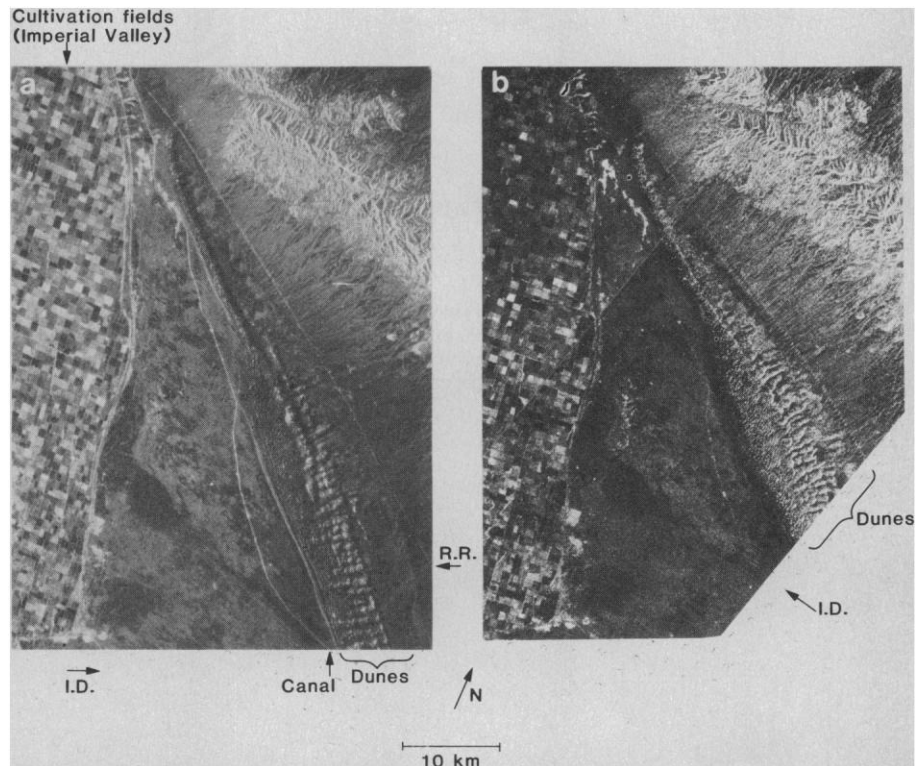


Fig. 5. Two radar images of the Algodones dunes, California (33°N, 115°W) taken from two different directions. The cultivated fields of the Imperial Valley are imaged as a checkerboard pattern on the left. The railroad (R.R.) (east of the dunes) and the water canal (west of the dunes) are imaged as bright linear features.

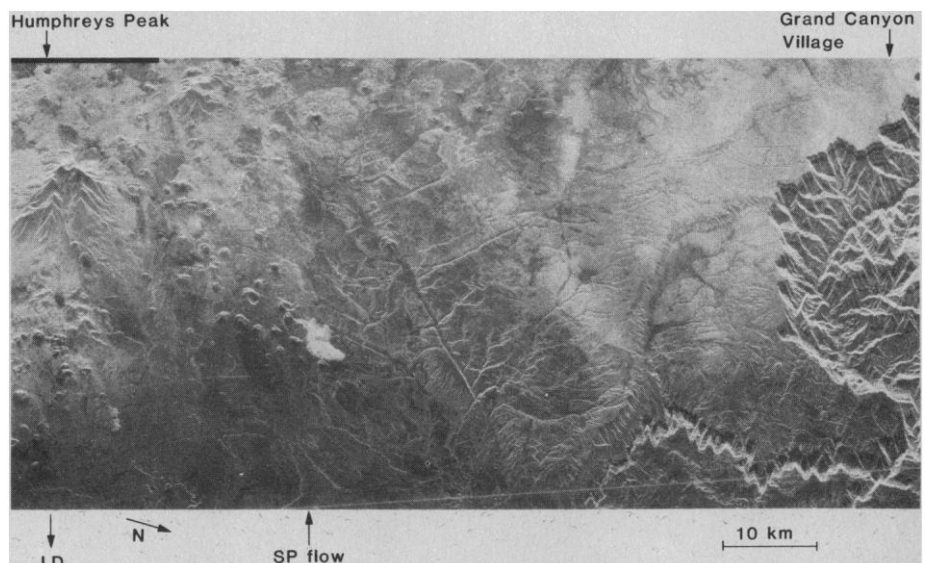


Fig. 6. Radar image of the south rim of the Grand Canyon (on the right part of the image) near Grand Canyon Village, and of the San Francisco volcanic field and Humphreys Peak (on the left part of the image). The location of the center of the image is 35°45'N, 111°30'W. The dark bands in the canyon wall correspond to the different strata which have a vertical slope and are therefore in shadow. The bright feature in the center of the image is the SP lava flow with its source, the SP cinder cone. Almost all the cinder cones in the area are identifiable on the image. The linear feature in the center of the image is the Mesa Butte graben (part of the Mesa Butte fault system).

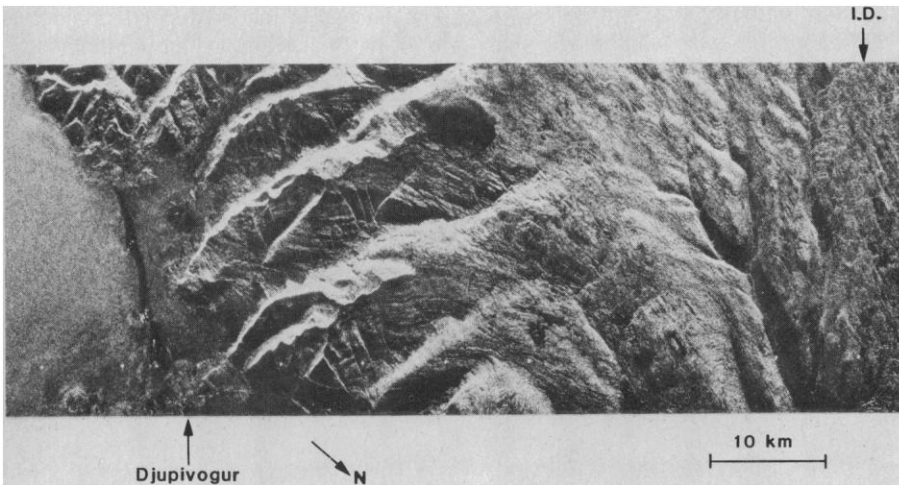
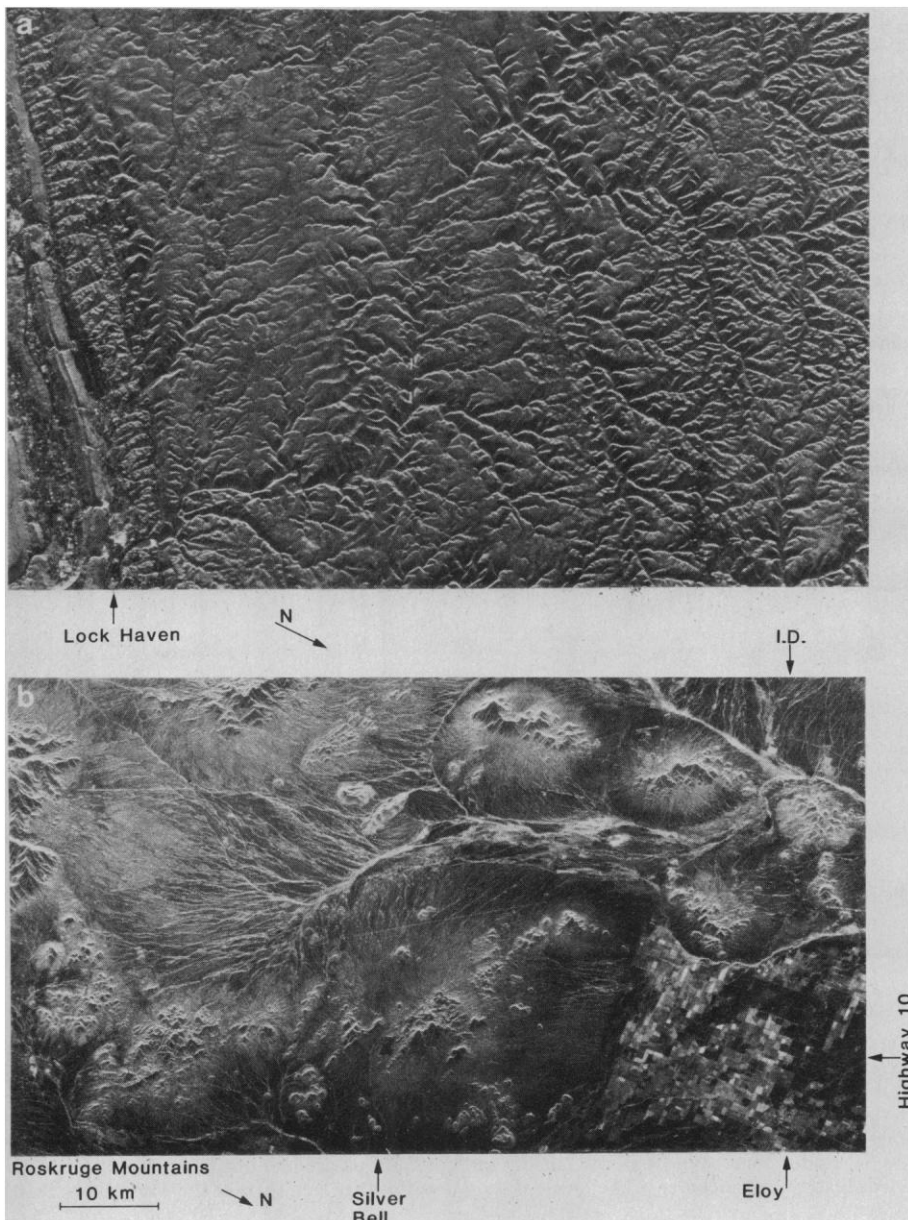


Fig. 7. Radar image of the Berufjordur region in eastern Iceland ($64^{\circ}40'N$, $14^{\circ}20'W$). The post of Djupivogur is at the lower left. Numerous strata on the north sides of the fjords are observed as bands of different tones. Strata as thin as 50 m can be observed. The mountain slopes facing the radar (facing south) are drastically distorted because of the foldover effect.



Specific determination of the rock type in each one of the different units would require additional information from multispectral infrared and visible sensors and ultimately from spot field measurements. Figure 9 shows an image of Death Valley, California, where the surface lithology is expressed in variations of the surface roughness. This is a situation that is particularly favorable for radar observation. Almost all of the geologic units that have been mapped as a result of field work (14, 19, 20) can be discerned on the radar image as tonal changes. In Fig. 3 also, variations in texture correlate well with variation in the rock type (15).

The radar images discussed in this section constitute a small sample of the types of geologic features that were observed with the Seasat SAR. Work is just beginning to assess the additional information that could be derived from this new type of data. The Seasat SAR had an observation geometry which was not necessarily the most favorable for geologic mapping. Future experiments, especially those in which the Space Shuttle is used as an orbiting platform, should allow us to assess the effects of the different radar sensor characteristics (that is, look angle, polarization, and frequency) on the information content of the images.

Oceanographic Applications

In oceanographic applications, the imaging radar sensor has a unique and essential characteristic: the capability of obtaining high-resolution surface images independent of the cloud cover and at any time of the day or night. It is essential because of the dynamic nature of almost all the features on the ocean surface. In actuality, the desired objective of oceanographic monitoring satellites is to be able to monitor, on a global basis, the ocean surface every few days.

The radar sensor provides an image

Fig. 8. Two examples of drainage patterns observed on the Seasat SAR images. (a) The Lock Haven region in Pennsylvania ($41^{\circ}N$, $78^{\circ}W$). Notice the change in the drainage pattern density in the Catskill Formation on the right part of the image relative to the Mississippian Pocono Group in the center part. The drainage channels are observed mainly because of their topographic expression. (b) The Silver Bell region, Arizona ($32^{\circ}30'N$, $111^{\circ}40'W$). Radial, centripetal, and annular patterns can be observed. The drainage channels are observed mainly because of the strong scattering from the vegetation along the channels.

that is representative of the surface backscatter characteristics. In the case of the ocean, the backscatter is completely controlled by the small-scale surface topography, the short gravity and capillary waves which scatter the radar energy by the Bragg scattering mechanism (21), and the local tilt of the surface, which is due to the presence of large waves and swells. Thus, the SAR is capable of imaging surface and near-surface phenomena that affect the surface roughness directly or indirectly. These phenomena include surface waves, internal waves, currents, weather fronts, wind or oil slicks, and eddies. Changes in surface temperature can be detected only if they affect the surface roughness. In this section, I briefly discuss examples of ocean features that have been observed with Seasat SAR. Verification of the observations on the radar image requires that surface observations be planned in advance and conducted simultaneously with the collection of radar data. Thus it is more difficult to verify ocean features than land features, which were observed on the Seasat SAR images.

Observations of ocean waves with airborne SAR were first reported by Brown *et al.* (6) and Larson *et al.* (7) in 1976. Since then, numerous other ocean features have been observed with airborne SAR sensors (6-9). However, aircraft observations are limited in aerial and temporal coverage, and the phenomena under observation are highly dynamic and variable. For the first time, the Seasat SAR provided a synoptic view of large ocean and ice-covered polar areas. In some cases, it also provided repetitive observations of the same region every 3 days.

Surface waves are visible on the radar image as a periodic regular change in the image tone (Fig. 10). The spatially periodic change in the surface-coherent backscatter cross section is a result of three surface effects that are modulated by the presence of a propagating surface wave or swell: (i) local slope, (ii) the intensity and bunching of the small gravity and capillary waves (22), and (iii) the wave orbital velocity, which affects the phase of the returned echo. The relative importance of these three effects is not yet well understood (10).

Figure 10 shows a Seasat image of ocean surface waves acquired over the northeastern Atlantic. In less than 5 minutes, the Seasat SAR provided an image of the Atlantic region between Scotland and Iceland 2000 km long and 100 km wide. In effect, it provided an almost instantaneous snapshot of the wave pat-

tern (wavelength and wave direction) in that region.

Internal waves. These waves are observed as a result of their surface manifestations and their effect on the surface roughness. The rather large currents associated with these waves modify the capillary-ultragravity surface wave spectrum overlying the oscillations. The exact mechanisms by which the modifications take place are still the subject of discussion, but at least two hypotheses have been advanced (23). According to the first hypothesis, the high velocity of surface water arising from the internal wave amplitude can sweep surface oils and materials together to form a smooth strip near regions of surface water convergence. The second mechanism predicts that capillary and ultragravity wave

energy is concentrated in the convergence zone by surface current stress, which then becomes a region of enhanced roughness rather than a smooth area as with the first hypothesis. When such smooth and rough regions are illuminated away from normal incidence and then viewed at nonspecular angles, the smooth region would appear darker and the rough one brighter than the normal sea surface. This geometry is the same for both imaging radar and multi-spectral (including optical) sensors.

Internal waves are usually observed on the radar image as a wave packet that consists of a series of convex strips, with the spatial periodicity becoming shorter toward the center of curvature (Fig. 11). The length of the crest may range up to many tens of kilometers. The leading

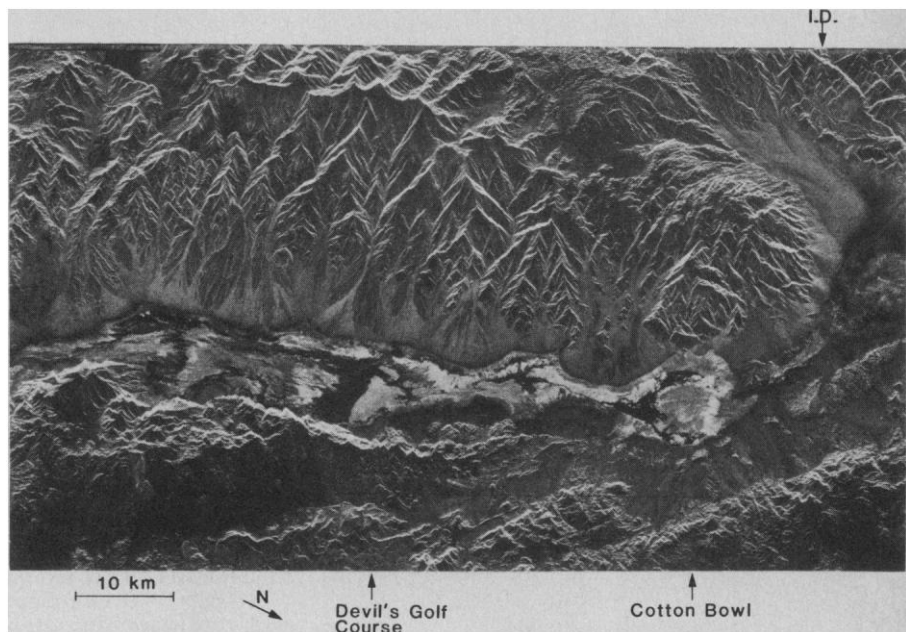


Fig. 9. Radar image of Death Valley, California (36°20'N, 116°50'W). The Cotton Bowl (silty rock salt) is the gray circular feature on the right. The dark continuous curvilinear band across the image corresponds to the edge of the alluvial fans at their intersection with the valley floor. The rough massive rock salt in the Devil's Golf Course shows a relatively bright tone.

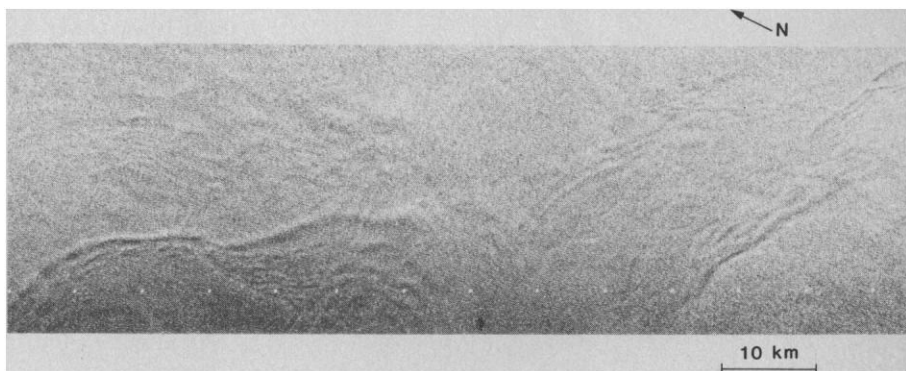


Fig. 10. Radar images of ocean surface waves in the northeastern Atlantic (60°N, 6°W, 19 August 1978). The swells have a wavelength of 400 m and are visible as a periodic tonal change. Other large-scale curvilinear features are also visible, some of which could be associated with internal waves. The ocean bottom depth in this area is between 100 and 500 fathoms.

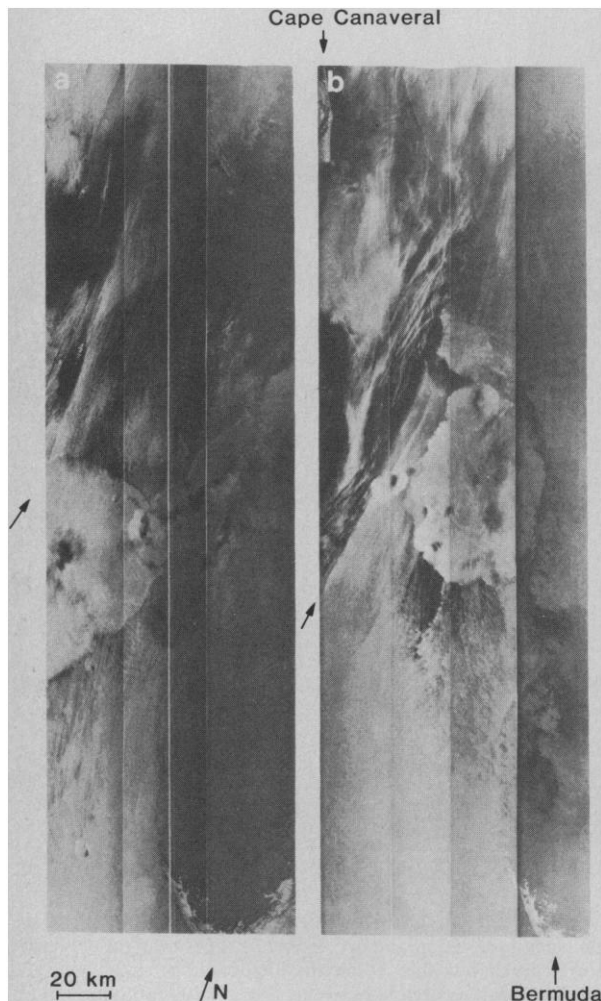
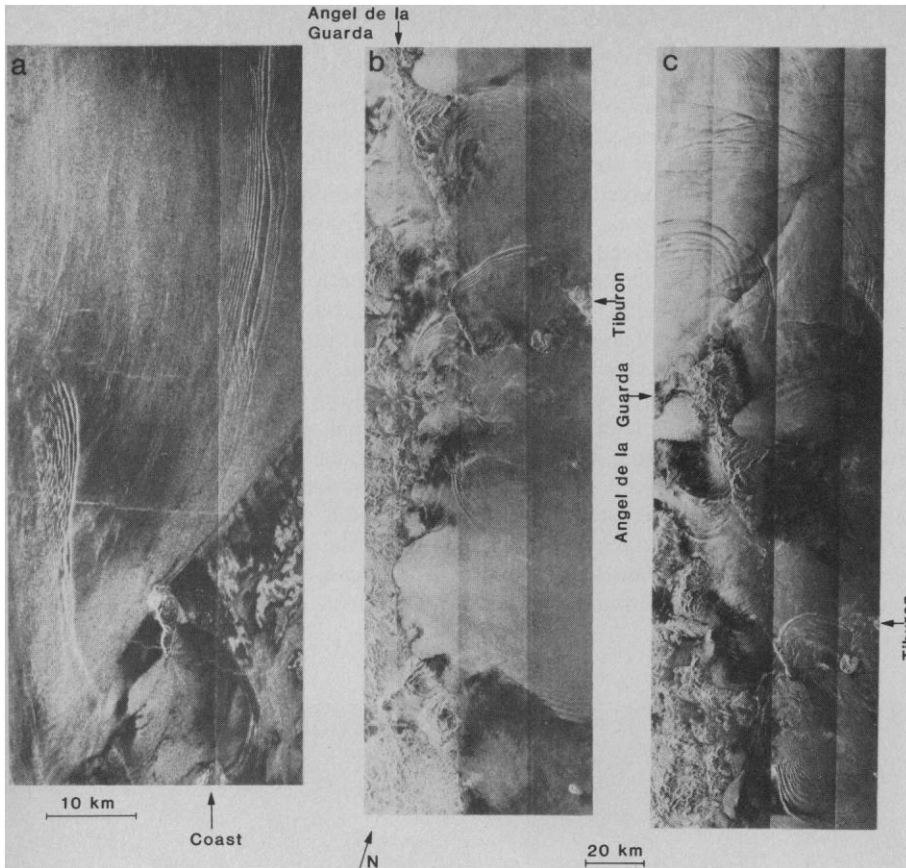


Fig. 11 (above). Radar images of groups of internal waves. (a) The western coast of Baja California (7 July 1978) near Isla Magdalena ($27^{\circ}50'N$, $115^{\circ}W$). (b) The Gulf of California off the coast of Baja California (14 September 1978) (upper part of image). The narrow long island in the center is San Lorenzo. (c) The Gulf of California (17 September 1978 at 17:20 G.M.T.) ($29^{\circ}N$, $113^{\circ}W$). Fig. 12 (left). Two radar images of the region between Grand Bahama Island (lower right corner) and the Florida coast. The images were taken on (a) 8 July 1978 and (b) 25 July 1978. The linear tonal change boundary, which is diagonal across the upper half of the images (indicated by an arrow) corresponds to the expected location of the western edge of the Gulf Stream.

wavelengths are on the order of 1 to 2 km and decrease monotonically toward the rear. They usually occur in groups or packets, and they have been observed in numerous places along the western and eastern coasts of North America. These waves are visible apparently because the surface stress is active in the front of a given cycle (leading to a rough surface and strong backscatter), which shows up as a bright tone, and is trailed by a slick formation, which exhibits a dark tone. Similar observations have been conducted with aircraft SAR (6-8) and optical sensors (24). On some Seasat single swaths, more internal waves could be observed than the total number observed during dozens of aircraft flights over a period of 5 years. This illustrates the new insight that resulted from the Seasat SAR experiment on the extent and rate of occurrence of certain dynamic ocean phenomena.

Figure 11a shows a group of internal waves along the west coast of Baja California, near Boca de la Soledad and Isla Magdalena. They appear as a succession of bright narrow convex strips separated by dark regions. The bright strips are about 100 m wide, and the wavelengths range from about 1 km at the front to about 100 m at the back of the wave. The fronts are usually a well-defined, long bright strip, whereas the backs sometimes consist of short, broken strips.

Figure 11, b and c, shows the surface patterns observed in the Gulf of California near the islands of Angel de la Guarda, Tiburón, and San Lorenzo. The two images were taken 3 days apart. In Fig. 11b, some internal waves are visible, particularly the two next to San Lorenzo. Their characteristics are similar to the ones discussed above. Figure 11c shows a very large number of what seem to be internal waves with a wide variety of linear scales. Some of the waves just northwest of Angel de la Guarda had wavelengths up to 5 km, had highly convex fronts, and were more than 40 km long. The wave pattern was characterized by dark narrow strips, about 500 m wide, separated by wide, relatively brighter regions. Some of these waves overlap, leading to interference patterns. The waves northeast of Angel de la Guarda and south of San Lorenzo have characteristics similar to the ones observed in Fig. 11, a and b.

The Gulf Stream. The northwestern Atlantic region was imaged numerous times to observe the surface features that are associated with the Gulf Stream. Figure 12 shows two radar images of the region between Grand Bahama Island and the coast of Florida (near Cape Canav-

eral) that were taken on 8 and 25 July 1978. No sea truth was obtained simultaneously with the radar observations. The linear boundary observed on both images corresponds closely to the expected location of the western edge of the Gulf Stream. The boundary in the image corresponds to an abrupt change in the image tone which corresponds to a change in the backscatter cross section. Numerous streaks in the same general direction as the boundary are also observed on the image, giving the impression of a flow. Possible explanations for the change in the backscatter return, and therefore image tone, include the following: (i) the water motion and temperature change lead to an abrupt discontinuity in the surface roughness which results in a change of the backscatter; or (ii) the abrupt change of the water motion leads to a differential Doppler shift in the returned echo which tends to create a bunching effect and a localized change in the image brightness at the boundary.

In Fig. 12b, a group of internal waves can be seen just off the coast of Cape Canaveral. In the same area, two vessels are visible as very bright point objects.

Polar sea ice. Mapping and large-scale

dynamics measurement of polar sea ice is another major application of SAR that is being investigated. Of particular interest is the capability of an orbiting SAR to monitor on a global and repetitive basis the dynamics, structure, and extent of the polar sea ice cover. Figure 13 shows two Seasat images taken 3 days apart over a region just north of Banks Island in Canada. Image tone variations and geometric shapes and forms enable one to identify floes and ridges in the floating ice and the open water. Many leads froze or closed during the 3-day period. Even though the ice patterns changed appreciably over that period, many individual ice floes could be identified and their motion determined. An ice movement of up to 15 km per day, on the average, has been measured on these images.

Conclusions

The Seasat SAR has provided large-scale radar images of land and ocean surfaces for the first time. A preliminary analysis of the data indicates that spaceborne imaging radar will improve our capability to assess earth resources and

monitor the ocean surface. It is expected that the radar sensor will add new types of information that will complement the geologic information presently being collected by optical and infrared sensors and by other conventional mapping techniques. The radar sensor is unique because it is capable of monitoring the ocean surface without environmental limitations. Much more work is needed to understand the geophysical information in the radar signature of different surfaces and to determine the optimum sensor characteristics (observation geometry, spectral coverage, polarization) for specific applications. The Space Shuttle is expected to be an appropriate platform for conducting such research, and experiments are being planned for the early 1980's that will use Shuttle imaging radar.

As with optical sensor data, the identification of different geologic units (and possibly ocean surface features) is more successful when multispectral observations are made. The L-band (wavelength about 25 cm) radar sensors, such as the one on Seasat, are most sensitive to roughness in the range from 2.5 to 25 cm. With the addition of an X-band (wave-

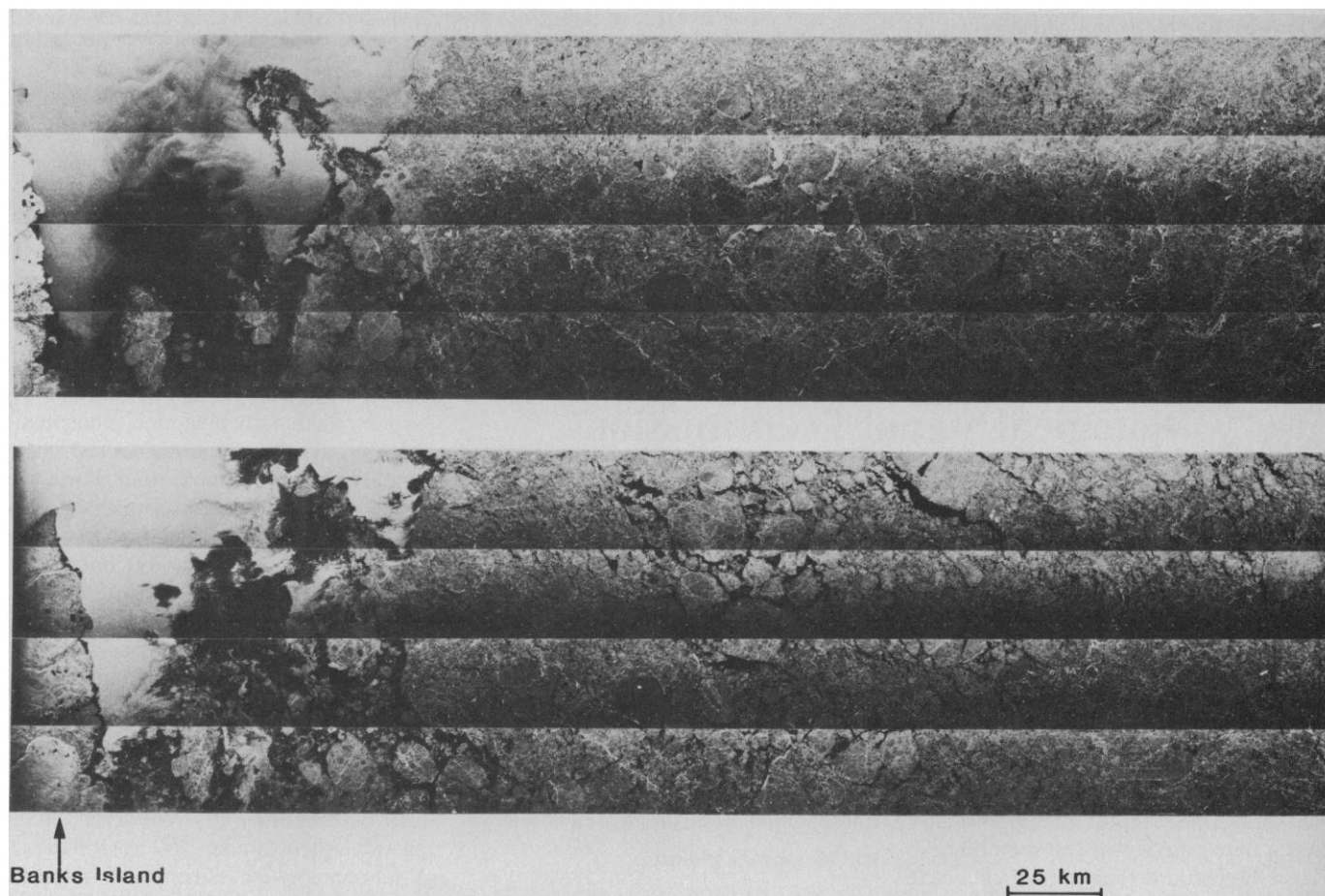


Fig. 13. Two radar images of a region of the Beaufort Sea, west of Banks Island in Canada ($72^{\circ}30'N$, $126^{\circ}W$), acquired 3 days apart in late September 1978. The northern shore of Banks Island is to the left with open water along it. The rest of the image covers a region of floating ice. Some individual ice floes can be identified on the two images; they have moved as much as 45 km in 3 days, and the ridges and lead patterns have changed as a result of the ice motion. The striping is an artifact due to mosaicking.

length about 3 cm), for example, the range of roughness sensitivity can probably be expanded to 0.3 to 3 cm, thus improving the discrimination capability (18, 20, 25). The development of a multispectral spaceborne radar system is expected to take place in the next few years.

Orbital radar will also allow us to develop a data base for the interpretation of images to be obtained from planetary missions. For Venus, and possibly Titan, radar will be the only means of mapping the planet's surface through the continuous and complete cloud cover.

Because of the complex nature of SAR's on orbital platforms, the successful development of the Seasat SAR was a key technical advancement. Major technological developments are still needed before multispectral orbiting SAR sensors can become operational, particularly in the area of digital, real-time processing. Because the radar sensor basically provides a Doppler time-delay history of each point target, thousands of computational operations are required to generate a single image element. This processing requirement, combined with the desire to have large swath mapping with high resolution, requires extremely fast processing hardware which is just at the limit of present-day technology.

References and Notes

1. G. H. Born, J. A. Dunne, D. B. Lame, *Science* **204**, 1405 (1979).
2. For a detailed review of the SAR principle, see the following: W. M. Brown and L. J. Porcello, *IRE Trans. Mil. Electron.* **MIL-6**, 111 (1969); L. J. Cutrona, in *Radar Handbook*, M. I. Skolnik, Ed. (McGraw-Hill, New York, 1970), p. 23.1; R. O. Harger, *Synthetic Aperture Radar Systems, Theory and Design* (Academic Press, New York, 1970); H. Jensen, L. C. Graham, L. J. Porcello, E. N. Leith, *Sci. Am.* **237**, 84 (October 1977).
3. K. Tomiyasu, *Proc. IEEE* **66**, 563 (1978).
4. In the case of the Seasat SAR, the illumination angle was fixed at 20°. Two illumination directions were possible, one during the ascending orbit and one during the descending orbit. The angle between these two directions varied from 0° to 144°, depending on the latitude of the area being imaged.
5. H. C. MacDonald, *Mod. Geol.* **1**, 1 (1969); R. S. Wing, *ibid.* **1**, 173 (1970); *ibid.* **2**, 1 (1971); *ibid.*, p. 75; _____ and L. Dellwig, *Geol. Soc. Am. Bull.* **81**, 293 (1970).
6. W. E. Brown, C. Elachi, T. W. Thompson, *J. Geophys. Res.* **81**, 2657 (1976).
7. T. R. Larson, L. I. Moskowitz, J. W. Wright, *IEEE Trans. Antennas Propag.* **AP-24**, 393 (1976).
8. C. Elachi, *J. Geophys. Res.* **81**, 2655 (1976); *Boundary Layer Meteorol.* **13**, 165 (1978); _____, T. W. Thompson, D. King, *Science* **198**, 609 (1977).
9. C. Elachi and J. Apel, *Geophys. Res. Lett.* **3**, 647 (1976).
10. C. Elachi and W. E. Brown, *IEEE Trans. Antennas Propag.* **AP-25**, 84 (1977); W. R. Alpers and C. L. Ruffenach, *ibid.* **AP-27**, 685 (1979).
11. For more information, see the following: W. J. Campbell *et al.*, *Boundary Layer Meteorol.* **13**, 309 (1978); F. Leberl, M. L. Bryan, C. Elachi, T. Farr, W. Campbell, *J. Geophys. Res.* **84**, 1827 (1979).
12. R. K. Moore, in *Manual of Remote Sensing*, R. G. Reeves, Ed. (American Society of Photogrammetry, Falls Church, Va., 1975).
13. V. C. Miller, *Photogeology* (McGraw-Hill, New York, 1961); R. G. Ray, *U.S. Geol. Surv. Prof. Pap.* **373** (1972); T. E. Avery, *Interpretation of Aerial Photographs* (Burgess, Minneapolis, Minn., ed. 3, 1977); F. F. Sabins, *Remote Sensing, Principles and Interpretation* (Freeman, San Francisco, 1978).
14. G. G. Schaber, G. L. Berlin, W. E. Brown, *Geol. Soc. Am. Bull.* **87**, 29 (1976).
15. J. Ford, *Am. Assoc. Pet. Geol. Bull.*, in press. For lineament mapping with Seasat SAR, see also F. F. Sabins, R. Blom, and C. Elachi [*ibid.* **64**, 619 (1980)].
16. Foreshortening refers to the fact that areas with a slope toward the radar sensor will be spatially shortened as compared to areas of the same size with a slope away from the radar sensor. Fold-over refers to the situation when two or more points on the surface are at exactly the same range distance from the radar. In this case the images of these points are superimposed. This situation usually occurs when imaging rugged terrain at a small look angle (12).
17. C. Elachi and T. Farr, *Remote Sensing Environ.* **9**, 171 (1980).
18. G. G. Schaber, C. Elachi, T. Farr, *ibid.*, p. 149.
19. Based on a geologic map by C. B. Hunt and D. R. Mabey, *U. S. Geol. Surv. Prof. Pap.* **494-A** (1966).
20. M. Daily, C. Elachi, T. Farr, G. Schaber, *Geophys. Res. Lett.* **5**, 899 (1978); *J. Photogramm. Remote Sensing* **45**, 1109 (1979).
21. M. W. Long, *Radar Reflectivity of Land and Sea* (Lexington, Lexington, Mass., 1975); G. R. Valenzuela, *Boundary Layer Meteorol.* **13**, 61 (1978).
22. J. W. Wright, *Boundary Layer Meteorol.* **13**, 87 (1978).
23. G. Ewing, *J. Mar. Res.* **9**, 161 (1950); A. E. Garrett and B. A. Hughes, *J. Fluid Mech.* **52**, 179 (1972).
24. J. R. Apel, H. M. Bryne, J. R. Proni, R. L. Charnell, *J. Geophys. Res.* **80**, 865 (1975).
25. L. F. Dellwig and R. K. Moore, *ibid.* **71**, 3597 (1966); L. Dellwig, *Mod. Geol.* **1**, 65 (1969).
26. This article represents the results of one phase of research carried out at the Jet Propulsion Laboratory, California Institute of Technology, under contract NAS7-100, sponsored by the Non-Renewable Resources Office, Office of Space and Terrestrial Applications, NASA. I thank M. Abrams, R. Blom, M. L. Bryan, M. Daily, T. Dixon, J. Ford, R. S. Saunders, and H. Stewart from Jet Propulsion Laboratory for their helpful discussions.

Phospholipid Methylation and Biological Signal Transmission

Fusao Hirata and Julius Axelrod

The mechanisms by which specific biochemical signals are transmitted through membranes is a problem of major importance in biology. Biochemical messages in the form of neurotransmitter, peptide hormone, lectin, and immunoglobulin ligands are recognized by and bind to specific receptor macromolecules on the outer surface of cell membranes. These interactions then initiate chemical and physical changes in membranes which in turn allow cells to carry out their specific function. Experiments in our laboratory in the past 3 years have

shown that enzymatic methylation of phospholipids play an important role in the transduction of receptor-mediated signals through the membranes of a variety of cells.

Phospholipid Methylation, Translocation, and Membrane Fluidity

We observed that the addition of Mg²⁺ ions to adrenal medulla homogenates stimulated the incorporation of the radioactive methyl group of S-adenosyl-L-

[methyl-³H]methionine (SAM), a methyl donor, into a lipid fraction (1). This prompted us to examine the identity of the [³H]methylated lipids, which we separated by extraction with organic solvents and by thin-layer chromatography. We found that the [³H]methyl groups were incorporated into phosphatidyl-N-monomethylethanolamine, phosphatidyl-N,N-dimethylethanolamine, and phosphatidylcholine. After further work, we found two enzymes in the adrenal medulla that converted phosphatidylethanolamine to phosphatidylcholine by successive methylations with SAM (1). Synthesis of phosphatidylcholine by two methyltransferases had been proposed previously (2) in genetic variants of the yeast *Neurospora crassa*.

The two phospholipid methyltransferases in the adrenal medulla have different properties (Fig. 1). The first enzyme (methyltransferase 1) converts phosphatidylethanolamine to phosphatidyl-N-monomethylethanolamine, requires

F. Hirata is a visiting scientist and J. Axelrod is Chief of the Section on Pharmacology, Laboratory of Clinical Science, National Institute of Mental Health, Bethesda, Maryland 20205.